# Ultra Wideband Channel Model for Indoor Environments

Alvaro Alvarez, Gustavo Valera, Manuel Lobeira, Rafael Pedro Torres, and Jose Luis Garcia

*Abstract:* **This paper presents an in-depth study of a ultra-wideband (UWB) indoor radio channel between 1 and 9 GHz, which was used for the subsequent development of a new statistical UWB multipath channel model, focusing on short range indoor scenarios. The channel sounding process was carried out covering different indoor environments, such as laboratories, halls or corridors. A combination of new and traditional parameters has been used to accurately model the channel impulse response in order to perform a precise temporal estimation of the received pulse shape. This model is designed specifically for UWB digital systems, where the received pulse is correlated with an estimated replica of itself. The precision of the model has been verified through the comparison with measured data from equivalent scenarios and cases, and highly satisfactory results were obtained.**

*Index Terms:* **UWB, channel model, channel impulse response (CIR), multipath, impulse radio channel, propagation.**

## I. INTRODUCTION

Recent years have seen the development of an innovative technology for short-range medium/high data rate communications. It has received several different names such as Impulse Radio, Baseband Radio, Pulsed Communications, though the most widely used name, which is ultra-wideband (UWB). All around the world the regulatory bodies, operators, industrial partners, academic researchers and standardization agencies are involved in the discussions that will lead to its regulation and to a UWB standard. Last year (February 2002), the FCC[1] published the first regulatory draft based on the work carried out over the previous four years, taking into account the impact or interference of UWB signals over other radio systems. This draft allows the operation of UWB systems mainly in the 3 to 10 GHz band, limiting the power level emission to -41 dBm/MHz. In Europe, the ETSI[2] has proposed a similar frequency mask for UWB devices.

The basis of the UWB systems is the transmission of the information through the radiation of sub-nanosecond pulses, which means, in the frequency domain, a spectrum of several GHz with low power spectral densities. These low PSD values, sometimes below the thermal noise floor of typical cellular systems, could solve the current saturation of the spectrum by enabling the sharing of already assigned bands with new UWB systems. Other important features of this technology are low complexity hardware structures, carrier-less architectures, low powered devices, accurate localization and multipath immunity [1].

Former studies on the UWB propagation channel were based on well-known wideband channel models, and include the advances achieved in this area during the last two decades. Two seminal works, among others, are those by Saleh-Valenzuela [2] and Hashemi [3]. One of the ideas behind the development of these classical models was their usefulness to understand and to simulate the impact of the radio-channel on wideband digital signals. Several reasonable assumptions were made: a) Some parameters derived from the knowledge of the power delay profile (PDP) are enough to have a first estimate of the impact of the channel on the signals, i.e., the RMS Excess Delay or the Coherence Bandwidth. b) In order to simulate accurately the effect of the channel on digital signals, a tapped delay line approach to the channel impulse response (CIR) is suitable. The number of taps or bins that form the discrete model of the CIR depends on the ratio between the CIR duration and the symbol period.

Recent works [4]–[7] have employed different techniques, both time and frequency domain, characterizing the channel through classical parameters employed in previous models not originally intended for bandwidths exceeding several GHz.

Within the European Union, and funded by the Information Society Technologies (IST) programme, the U.C.A.N.[3] project is aimed at the implementation of a wireless UWB Impulse Radio system for short-range high bit rate communications. This paper summarizes part of the work carried out within this project, in order to characterize and model the UWB propagation. We propose a different model approach, based on frequency domain measurements (as reported in [4]–[9]), performing real passband signal processing [4], defining new model parameters not yet employed in any previous channel model (ZCR), and not including classical parameters such as RMS delay spread or excess delay.

In this paper we present a new model for UWB that takes into account the peculiar nature of UWB systems and the clear differences with classical modulated or passband radio systems. Thus, the proposed model differs from the previous ones in the following aspects: a) The main magnitude is the real passband CIR [4] rather than the complex baseband CIR [2], b) classical parameters as RMS delay spread or coherent bandwidth have little or no value at all, since they are not considered in the framework of this new model. For this reason, a new statistical model capable of reproducing the full waveform of the CIR is proposed. This model is more suitable than a discrete multi-bin approach due to the big number of bins needed in the latter, because of the long duration of CIR with respect to the UWB pulse duration.

Manuscript received June 30, 2003, November 13, 2003.

Alvaro Alvarez is with ACORDE.SA, CDTUC, Av. Los Castros s/n, Santander, Spain, email: alvaro@acordecom.com.

Gustavo Valera, Manuel Lobeira, Rafael Pedro Torres, and Jose Luis Garcia are with the University of Cantabria, at the Communications Department (DICOM), Av. Los Castros s/n, Santander, Spain, email: {gvalera, mlobeira}@dicom.unican.es, torresrp@unican.es, jlgarcia@dicom.unican.es.

This work was supported in part by the European Commission, under the project U.C.A.N. (IST-2001-32710).

[1] Federal Communications Commission.

[2] European Telecommunications Standard Institute.

[3] Ultra-wideband concepts for ad-hoc networks.

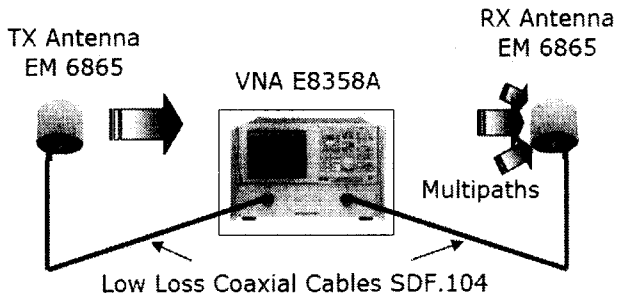


Fig. 1. Measurement set-up schematic.

The first part of the paper describes the measurement methodology, laboratory equipment characteristics and configuration, as well as the different scenarios where the sounding process took place. Then, the data post-processing with all the mathematical approaches and algorithms applied are explained. Finally, the simulation results, together with their comparison with the real measurements, are presented.

## II. MEASUREMENT SETUP

Radio[4] channel measurements can be made in the time domain or in the frequency domain. Two of the most widely used techniques are: i) Recording the received pulse shape in the time domain using a pulse generator plus a high speed oscilloscope, ii) recording the channel transfer function, $H(f)$, in the frequency domain using a vector network analyzer (VNA) [4]–[6]. For our purposes the latter technique has been found to be more suitable. The VNA generates a sequence of $N$ frequency tones in the measured bandwidth (from $f_1$ to $f_N$), radiates them to the air through UWB antennas, and then records the received amplitude and phase from each tone (the VNA measures the $S_{21}$). This parameter includes both the channel and antenna response from which, making use of the Fourier Transform, the channel impulse response (CIR) in the time domain can be obtained.

The scheme in Fig. 1 gives a general overview of the main components of the measurement set-up. The output of the VNA on port 1 is connected to the biconical antenna through a low loss coaxial cable (10m long), and the received signal is captured by a second biconical antenna and fed into the port 2 of the Analyzer. Every sweep is recorded into different data files and saved in a PC.

This configuration employs a very simple architecture, but considering the measured environments it proved more than sufficient, since the dynamic range of the VNA and the large signal to noise levels made it unnecessary to use any active device (amplifiers). The lack of amplifying stages in the set-up chain helped us to avoid distortions, enabling the easiest calibration to be performed simply with a through-response. This calibration procedure is carried out at the cables front-end (the calibration includes the cables) but the antennas are included in the measurement (this is why the measured channel is called radio-channel rather than propagation-channel).

The VNA allows 1601 complex tones to be recorded for each sweep. The measured bandwidth was between 1 and 9 GHz, split in two sub-bandwidths measured consecutively (due to the temporal stability of the channel [7] within fixed scenarios), the first between 1 and 5 GHz, and the second between 5 and 9 GHz. Finally a single file with the recorded data between 1 and 9 GHz, and 3201 points is obtained. The Tx-Rx distances ranged from 1 to 18 meters, the observed channel was very slowly time-varying and the minimum SNR was 25 dB. Table 1 shows the technical characteristics, parameter values and a brief description of the VNA configuration for the measurement process.

[4]Radio channel means that the antenna effect is included in the measurement.

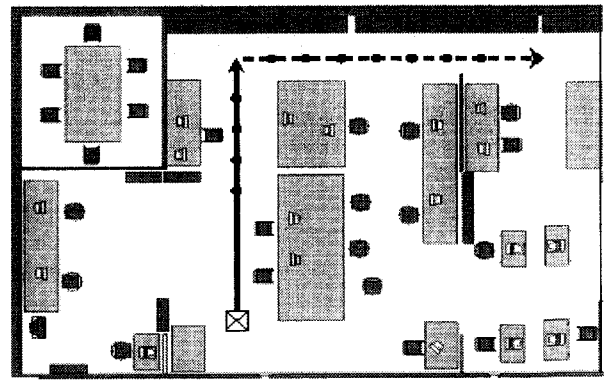

Fig. 2. Scenario 1 - laboratory.

Table 1. Measurement set-up summary.

| Device | Characteristics | |
|---|---|---|
| **Vector Network Analyser** | Model: | Agilent E8364A |
| | Operational range | 45MHz –50 GHz |
| | Internal IF settled: | 0.5 KHz |
| | Number of points: | 1601 |
| | Calibration type: | Through response |
| | Noise floor: | -99 dBm |
| | Output Power: | 6 dBm |
| | Output Data: | $S_{21}$ parameter |
| **Cables** | Type: | Low loss cable SDF.104 |
| | Loss: | 0.3dB/m @ 1 GHz, 0.33dB/m @ 9 GHz |
| | Connector: | N-type / SMA |
| **Antenna** | Model: | Electrometrics EM 6865 wideband. |
| | Frequency band: | 1-18GHz |
| | Gain: | - 0.9dBi @ 1 GHz 4.9dBi @ 9 GHz |
| | Polarization: | Vertical |
| | Impedance: | 50 Ω |

## III. SCENARIOS

Scenario is defined as the site where the measurements were taken and is characterized by the furniture, walls, area and other physical parameters, all of them with a strong influence on the channel response. There are four different scenarios covered in this work, three of them inside a laboratory building and the other one in an office block. All were indoor environments surrounded by typical office and laboratory furniture such as tables, chairs or shelves, and open areas were no bigger than 100 square meters.

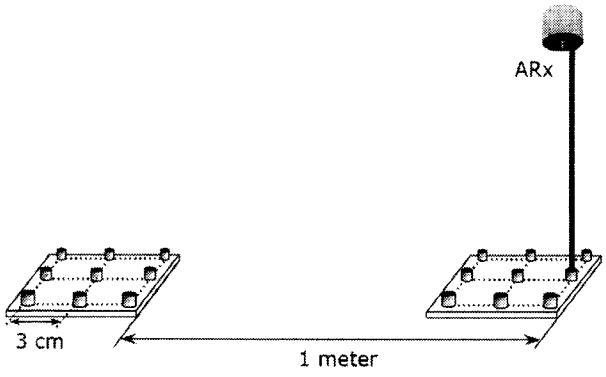


Fig. 3. Measured positions and small scale grid.

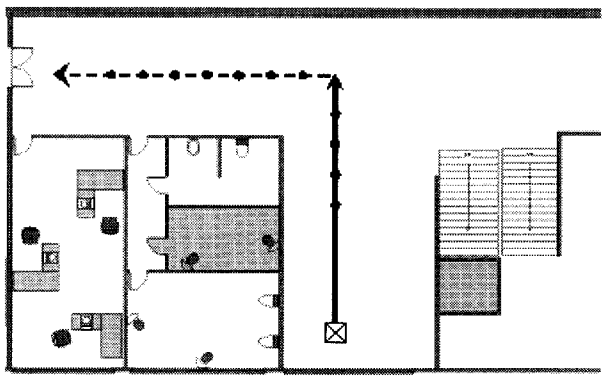

Fig. 4. Scenario 2 - CDTUC corridor.

### A. Scenario 1

This is found on the second floor of the laboratory building, and two types of measurements were performed, the first with direct line of sight between the Tx and Rx antenna (LOS), and the second one without line of sight (NLOS). Fig. 2 shows a diagram of the area indicating the exact points where the antennas were set, starting with a separation distance of 4 meters between them.

The transmitter antenna (ATx) is fixed in the same place for the whole process, and the receiver antenna (ARx) is moved through the scenario. From the first measured position, located at 4 meters, consecutive positions are placed every one meter, up to 18 meters of distance. Another important point is that at every position 9 measurements were taken over a grid of 3 by 3 points, with 3 cm separation among them, as shown in Fig. 3.

The following table (Table 2) describes the furniture and environment inside scenario 1 and its main characteristics.

### B. Scenario 2

This scenario comprises the corridor of the second floor of the laboratory building and includes both LOS and NLOS cases. The initial distance between ATx and ARx was 4 m again, and the measurement procedure follows the same methodology as in scenario 1.

Table 3 summarizes the main features of scenario 2, such as furniture in the scenario, open area, or type of walls.

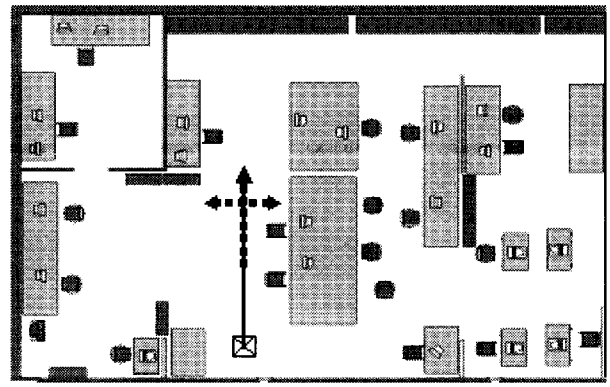

Fig. 5. Scenario 3 - laboratory floor 1.

Table 2. Scenario 1 main characteristics.

| **Scenario** | 1 - CDTUC Laboratory |
|---|---|
| **Area** | $\sim 100m^2$ |
| **Furniture** | Tables, shelves, chairs, PCs, electronic instrumentation $\cdots$ |
| **Antenna Separation** | $4 - 18m$ |
| **Measurement Type** | LOS and NLOS |
| **Number of Points** | $18 \times 3 \times 3 = 162$ |
| **Wall Type** | Internal: Plaster boards<br>External: Concrete & Windows |

Table 3. Scenario 2 main characteristics.

| **Scenario** | 2 - CDTUC Laboratory |
|---|---|
| **Area** | $\sim 60m^2$ |
| **Furniture** | No Furniture |
| **Antenna Separation** | $4 - 12m$ |
| **Measurement Type** | LOS and NLOS |
| **Number of Points** | $12 \times 3 \times 3 + 6 \times 3 \times 3 = 162$ |
| **Wall Type** | Internal: Plaster boards<br>External: Concrete & Windows |

### C. Scenario 3

On the first floor of the laboratory building, 500 points were measured with a distance from the ATx to the ARx between 1 and 4 meters (LOS, short range measurements), with separation between points of 1 cm. The measurements were taken at various points on a cross sized $3 \times 2$ meters (100 points/m).

### D. Scenario 4

This scenario is located at the University Polytechnic School, and it is a narrow corridor surrounded by walls, doors and bookshelves. There is Line of Sight (LOS) between ATx and ARx, and the separation between antennas varied from 4 to 11 meters, employing 1 meter steps in a $3 \times 3$ cm grid. Fig. 6 shows a description of the measured points, the cross represents the ATx, and the circles mark the positions of the center of the grid.

A brief summary of the main characteristics of scenario 4 is shown in Table 4.

## IV. DATA POST-PROCESSING

Considering the calibration process explained in Section III, the recorded data from the VNA, which consists of the $S_{21}$ parameter values, correspond to samples of the Channel Transfer

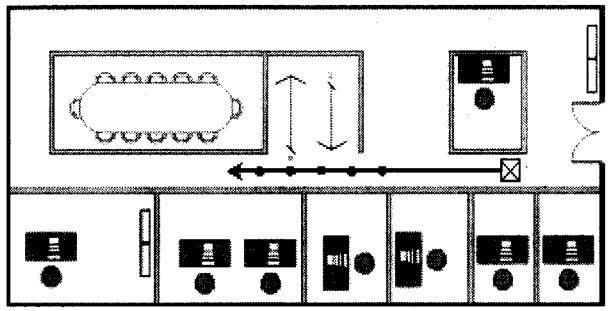

Fig. 6. Scenario 4 - corridor.

Table 4. Scenario 2 main characteristics.

| Scenario | 4 - Corridor |
|---|---|
| Area | $\sim 60m^2$ |
| Furniture | Bookshelves |
| Antenna Separation | $4 - 11m$ |
| Measurement Type | LOS |
| Number of Points | $8 \times 3 \times 3 = 72$ |
| Wall Type | Internal: Plaster boards<br>External: Concrete & Windows |

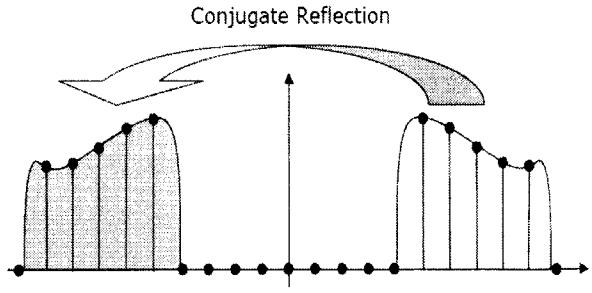


Fig. 7. 0-padding and hermitical symmetry.

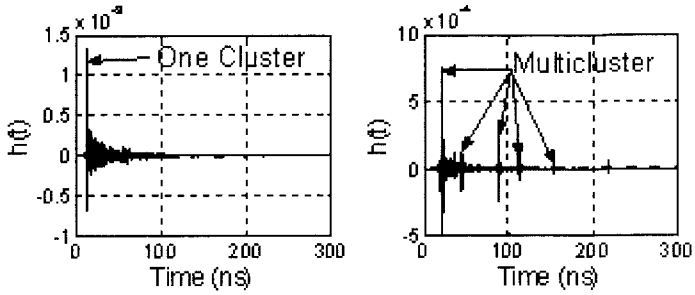


Fig. 8. Channel impulse response.

Function. This is a complex data vector,

$$H(k\Delta f) = Re[H(k\Delta f)] + jIm[H(k\Delta f)], \quad (1)$$

with a frequency step defined by the measurement process of:

$$\Delta f = \frac{f_{\mathrm{MAX}} - f_{\mathrm{MIN}}}{N-1}, \quad (2)$$

where $N$ is the number of recorded points. From the frequency domain data it is possible, by means of the inverse fast Fourier transform (IFFT), to obtain the channel impulse response (CIR), in the time domain:

$$h(n\Delta t) = \mathrm{IFFT}[H(k\Delta f)]. \quad (3)$$

Usually the IFFT is directly applied to the $H(k\Delta f)$ measured data without performing any translation of the points in the discrete frequency domain. This method is sometimes called the complex base-band IFFT and allows the lowpass equivalent CIR, which is a complex function, to be obtained. From the low-pass equivalent CIR the power delay profile (PDP) is directly obtained by calculating its module. In previous wideband models the major parameters describing the channel in the time domain were based on the knowledge of the PDP, for instance, the mean excess delay and the RMS delay spread.

In the UWB case, the interest is placed on the characterization of the received pulse, thus, the main magnitude is the RF CIR, a real function, rather than the lowpass equivalent CIR (complex). Therefore, a hermitical signal processing is required in order to obtain the channel impulse response (CIR). From the original measured data record, the hermitical pass-band signal is obtained by 0-padding from DC to the lower measured frequency value ($H(f_{\mathrm{MIN}})$) and adding the conjugate reflection up to the highest negative frequency [4].

With this processing methodology, the number of points of the information vector is doubled. In the frequency domain three parameters have to be established for processing:

- Frequency Range: $[f_{\mathrm{MIN}}, f_{\mathrm{MAX}}] = [1\ \mathrm{GHz}, 9\ \mathrm{GHz}]$
- Frequency Resolution: $\Delta f = 2.5$ MHz
- Total Number of Points: $N = 3201$

And, in the time domain the variables obtained are:

- Time resolution: ts=$\frac{1}{2f_{\mathrm{MAX}}} = 55$ps
- Total Time Response: $T = \frac{1}{\Delta f} = 400$ ns

The frequency range corresponds to the start and stop frequencies of the sweep cycle programmed in the VNA. The number of points is the number of tones of the measured vector, while the frequency step is the sweep range divided by the number of points. Also, the time resolution is the time interval between two consecutive samples in the IFFT vector, and the response duration is the time length of the $h[n\Delta t]$. The real passband method presented above, gives the real channel impulse response not the envelope of the complex baseband approach.

## V. UWB CHANNEL MODEL

Since we started our work on UWB channel modeling, many papers dealing with this important topic have been published. Many of them are based on previous (widely recognized) narrowband or wideband models. However, due to the special characteristics of the UWB pulsed signals and the receiver architecture proposed in the UCAN demonstrator, we decided to start a new model approach, having some similarities to previous models in certain aspects, but big differences in others.

We propose a channel impulse response (CIR) model, based on clusters. In our cluster approach, the multipath components are divided into two branches, and each cluster combines several multipath responses that are close in time, following a decaying law. One, a few or many clusters separated in time define the

Table 5. Decaying factor statistics.

| SCENARIO | $\gamma[ns-1]$ | |
|---|---|---|
| | $E[\gamma]$ | $\sigma[\gamma]$ |
| **LOS** | 0.010 | 0.021 |
| **Soft-NLOS** | 0.008 | 0.018 |
| **Hard-NLOS** | 0.006 | 0.023 |

complete multipath channel response. Fig. 8 presents and example of these two responses.

### A. *Time Domain Parameters*

The characterization, and future modeling of the channel time response, is based on four different parameters extracted from the power delay profile (PDP). Since the behaviour of the channels differs a lot depending on the environment, the best way to approach the characterization is through statistical analysis. This implies presenting the mean value and standard deviation, or directly the probability density function (pdf) that best matches the whole set of environment responses. The following paragraphs present these parameters as well as the results obtained.

▶ *Decaying factor,* $\gamma$ : This is the exponential approximation of the mean level of the PDP (linear in dB). The statistical behaviour is represented by a mean value and its standard deviation.

$$\overline{|h(t)|^2} = ke^{-\gamma t}, \tag{4}$$

$$\begin{aligned} 10\log_{10}\left(\overline{|h(t)|^2}\right) &= 10\log_{10}\left(ke^{-\gamma t}\right) \\ &= 10\log_{10}(k) + 10\log_{10}\left(e^{-\gamma t}\right) \\ &= K + 10(-\gamma t)\log_{10}(e). \end{aligned} \tag{5}$$

From recorded measurements and an adequate least square linear fitting process in Matlab, the mean and standard deviation values of this parameter for the different scenarios can be shown in the Table 5.

All the standard deviations remain within the same range of values, whereas the mean value decreases as the path gets more obstructed (from LOS to Hard-NLOS).

▶ *Power Variations,* $\chi$: Represents the power variations over the mean value in the PDP, and will be characterized by its probability density function (pdf).

$$|h(t)|^2 = ke^{-\gamma t} + \chi, \tag{6}$$

hence,

$$\chi = |h(t)|^2 - \overline{|h(t)|^2}. \tag{7}$$

For each PDP, we have obtained the histogram of these power variations values in order to estimate the most accurate probability density function (pdf) approximation. The histogram is a graphical tool developed by statisticians to visualize frequency distributions; it shows the discrete values of a pdf (which is a continuous function).

Another difference with other models is that the histogram is performed along the time axis and not along the distance axis.

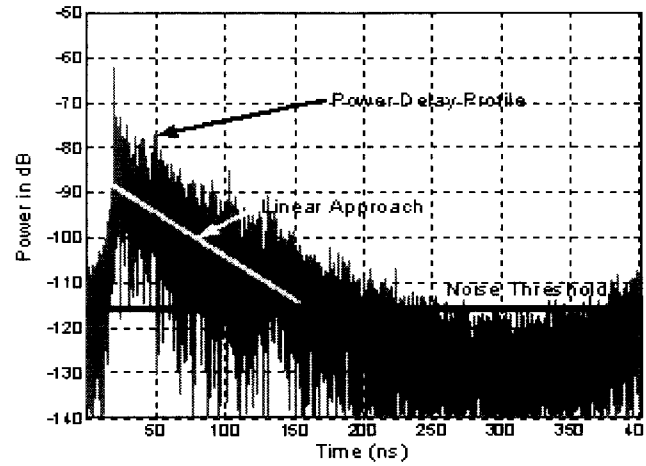


Fig. 9. Decaying factor.

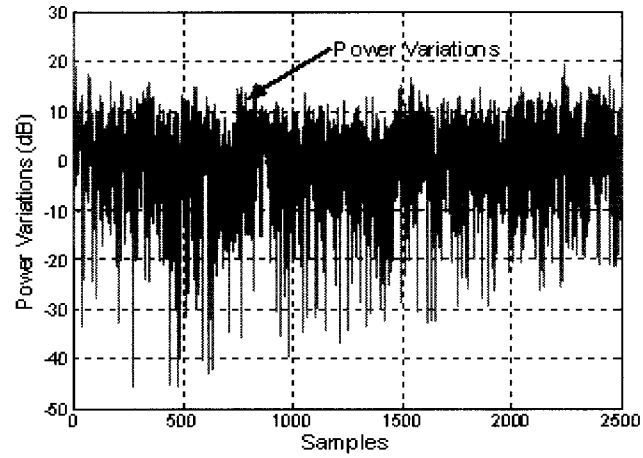


Fig. 10. Power variations over the linear cluster approach.

To compute the histogram along the distance axis, several (thousands) measurements in close scenarios (at least similar characteristic areas) are needed. However, the pdf computed along the time axis has demonstrated a good behaviour in the channel model results and far fewer measurements are required.

The bars are from the histogram while the bold line is the pdf approximation, a Weibull probability density function, whose formula has the following expression [10]:

$$f(x;\sigma;\lambda) = \frac{\lambda}{\sigma}\left(\frac{x-\mu}{\sigma}\right)^{\lambda-1}\exp\left\{\left(\frac{x-\mu}{\sigma}\right)^{\lambda}\right\}, \quad x \geq 0;\ \sigma,\lambda > 0. \tag{8}$$

The values for these parameters vary slightly for each different scenario, as can be seen in the following table.

These results have been obtained after the fitting process performed by a Least Squared method, leading to the lowest error on a Weibull curve approach. It is easy to verify that there is not much difference between the results for the three scenarios, which means that the power variations have a homogeneous behavior over all the analyzed scenarios.

▶*Cluster Hard Decay Time,* $\tau_H$: Is the approximated duration of the strongest part of the cluster. Particularly in LOS and Hard-NLOS (Hard-NLOS is when there is no direct or reflected

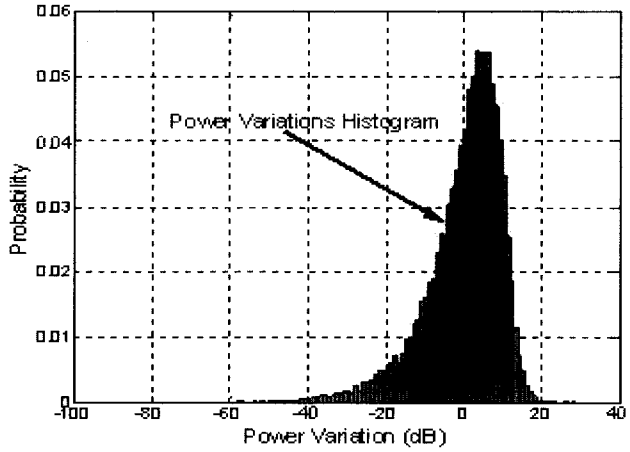


Fig. 11. Histogram of the power variations.

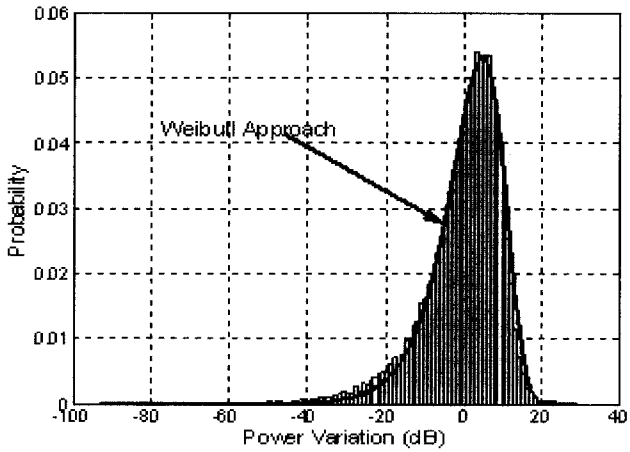


Fig. 12. Power variations histogram and the Weibull aprroximation.

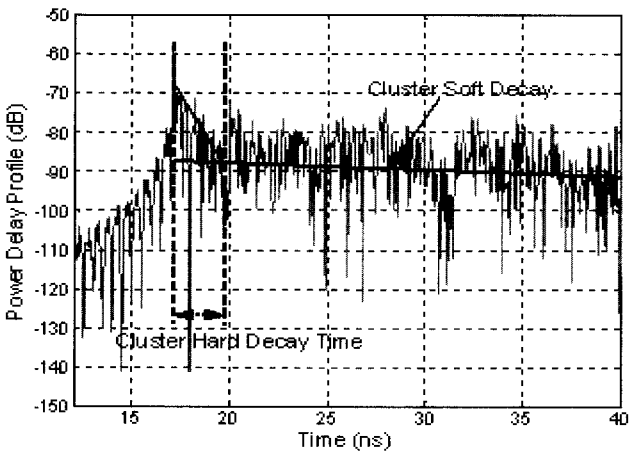


Fig. 13. Cluster time structure.

path between Tx and Rx, i.e., between two different rooms), each received cluster has got a strong component, belonging to the first (direct) path, and a weak tail due to other multipath contributions.

In Fig. 13, the Cluster Hard Decay Time (H) line represents the higher decaying slope which occurs within the cluster hard decay time, whereas the other line, the more gradual slope, belongs to the rest of the PDP duration. The statistics of H, extracted from the measurement campaigns are collected in the following table.

Table 6. Power variations pdfs.

| SCENARIO | $\chi$ | | |
|---|---|---|---|
| | $\mu$ | $\Sigma$ | $\lambda$ |
| **LOS** | -306 | 311 | 45 |
| **Soft-NLOS** | -304 | 320 | 46 |
| **Hard-NLOS** | -304 | 322 | 45 |

Table 7. Decaying factor statistics.

| SCENARIO | $\tau_H\,[ns]$ | |
|---|---|---|
| | $E[\tau_H]$ | $\sigma[\tau_H]$ |
| **LOS** | 2.32 | 0.82 |
| **Soft-NLOS** | 5.26 | 2.68 |
| **Hard-NLOS** | 4.02 | 1.54 |

As was expected, the shorter value is obtained for the LOS case, where the direct path keeps the highest energy portion. Meanwhile, the rest of the cases present a higher energy spread.

▶ *Zero Crossing Rate (ZCR)*: Represents the time that consecutive samples of the CIR kept the same sign (positive or negative). This is an essential source of information for the purpose of the UWB receiver final simulations. Also, in this case, the pdf has been obtained.

For this fourth parameter, it is necessary to differentiate two distinct temporal regions, which will be modeled separately. The first region covers PDP components up to the cluster hard decay time ($\tau_H$), while the second one starts at that time and lasts until the end of the PDP. The following figure represents the two pdf's obtained for the two temporal regions.

### *B. Frequency Domain Parameters*

▶ *Frequency Range*: Determined by the measured range. In our case three frequency ranges have been covered, in three different channel sounding campaigns.

- 1st CSC: 2 – 6 GHz
- 2nd CSC: 1 – 9 GHz
- 3rd CSC: 1 – 13 GHz

The explanation of the bimodal pdf for the first case is very simple. It has the common exponential behavior, but on top of this it presents the peculiarity of the main path (direct ray) influence, which provokes a higher probability of several consecutive samples keeping the same sign.

▶ *Frequency Decaying Factor, $\delta$ (delta)*: This is the exponential approximation in dB of the mean level of the Channel Transfer Function (linear in log scale). Its statistics are represented by the mean value and its standard deviation.

$$\log_{10}\left(\overline{|h(t)|^2}\right) = k_{H(f)}e^{-\delta f}. \tag{9}$$

This parameter is highly dependent on the antenna specifications. In our case two biconical broadband antennas were used, with a small ripple between 1 and 18 GHz. In the middle of the

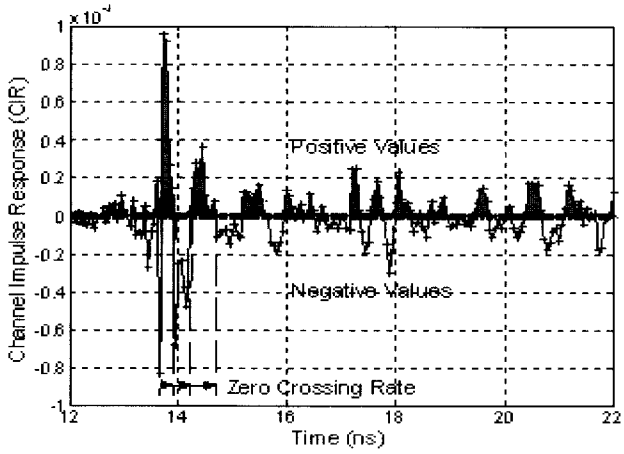


Fig. 14. Zero crossing rate representation.

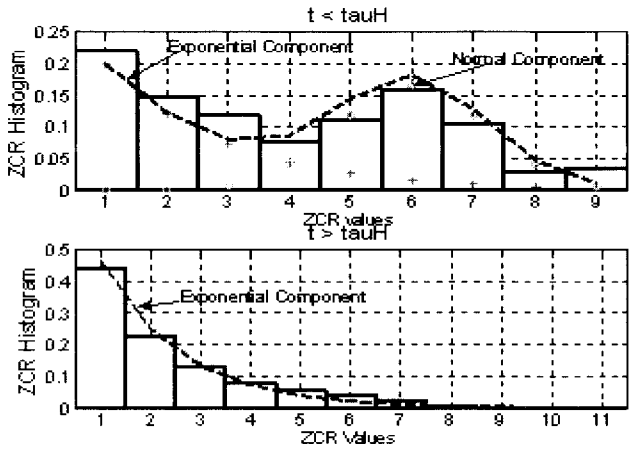


Fig. 15. PDF of the ZCR.

Table 8. $\delta$ statistics.

| SCENARIO | $\delta$ | |
|---|---|---|
| | $E[\delta]$ | $\sigma[\delta]$ |
| **LOS** | 1.01 | 0.18 |
| **Soft-NLOS** | 1.16 | 0.21 |
| **Hard-NLOS** | 1.36 | 0.24 |

Table 9. n statistics.

| SCENARIO | $d_0$(cm) | n | |
|---|---|---|---|
| | | E[n] | $\sigma[n]$ |
| **LOS** | 15.1 | 1.4 | 0.35 |
| **Soft-NLOS** | 8.2 | 3.2 | 1.21 |
| **Hard-NLOS** | 6.7 | 4.1 | 1.87 |

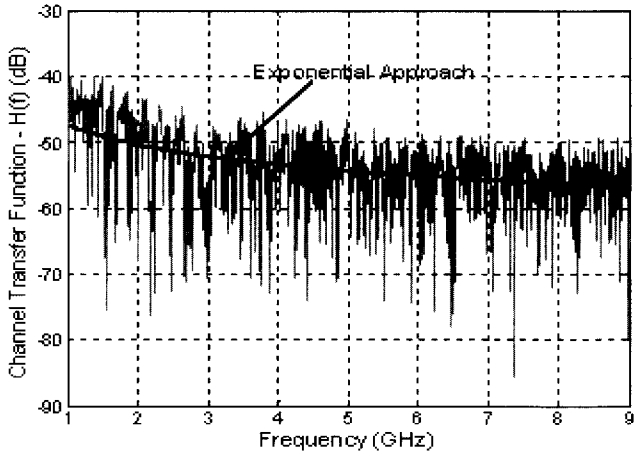


Fig. 16. Measured channel transfer function.

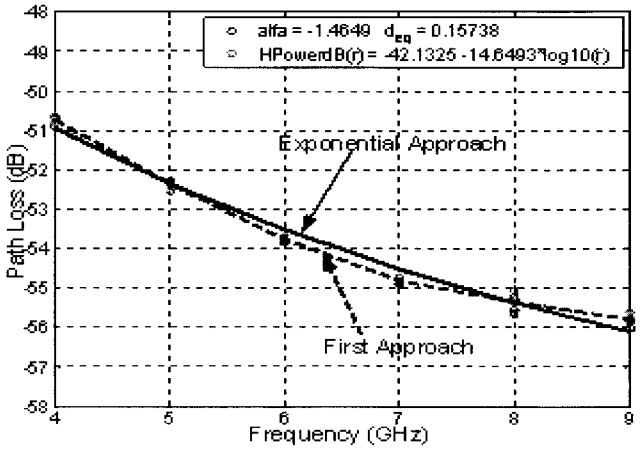


Fig. 17. Path loss exponent curve.

bandwidth (9 GHz), the gain is 3 dB while in the lower band (1GHz), it is -1 dB. This is why the $\delta$ parameter is not equal to two (2) as it should have been with an isotropic radiation pattern.

▶ *Path Loss Exponent (n)*: The path loss model follows the well-known lognormal shadowing effect around the mean value. For the mean value calculation, we assume an exponential variation of the received power with the distance [9].

$$L = L_{FS}(d_0) + 10n\log_{10}\left(\frac{d}{d_0}\right). \qquad (10)$$

The average value of $d_0$ and the statistical behavior of '$n$', characterized by its mean value and the standard deviation are included in Table 9.

Fig. 17 represents the received power in dBm as a function of the distance expressed in metres.

Since the reference distance ($d_0$) is assumed to be the limit up to which there is free space propagation, it is logical to have a decreasing value as the path finds more and more obstructions. Besides, these obstacles force the increasing value of '$n$', as our results shows.

## VI. UWB CHANNEL MODEL SIMULATION

In order to perform the simulation of the indoor channel between two UWB devices, separated at a distance '$d$', it is necessary to choose one scenario case from among the following ones: LOS, Soft-NLOS, Hard-NLOS or corridor. Once this step is completed, the simulation process will follow a set of different stages, in order to obtain the final channel impulse response.

### A. LOS Case

This is the case when there is a direct path between transmitter (Tx) and receiver (Rx), because both are located in an open area.

*Cluster positioning*: In LOS cases, as a first approximation, only one strong cluster will be considered, due to the assumption that other weak clusters exist, but they are below the first cluster tail (this is a first approach for LOS cases).

*PDP cluster generation*: The linear approximation of the power delay profile is generated taking into account the ($\gamma$ = Time domain decaying factor) parameter. Then, a second linear component representing the cluster hard decay time is added from $t = 0$ to $t = \tau_H$, and finally the power variations, represented by $\chi$ are applied .

*CIR-h(t) cluster generation*: The modulus of the CIR-$h(t)$ is obtained by the square root of the randomly generated PDP cluster. Then, the zero crossing rate probability density function is used to give the sign to the $|h(t)|$.

*CIR-h(t) complete response*: Considering that in LOS cases only one cluster is generated, the complete channel impulse response is just this cluster. Zero padding at the beginning of the vector can be performed in order to implement the channel delay due to the distance between the Tx and the Rx.

*CTF-H(f) frequency correction*: From the generated $h(t)$, via Fourier Transform, its correspondent channel transfer function can be obtained. The next step is to fit this data to the original conditions of the measurement process, that means, the frequency range (there can not be signal below $f_{\mathrm{MIN}}$ or above $f_{\mathrm{MAX}}$, because the model parameters have been obtained with this assumption), and to fit the frequency decaying factor to the parameterized one.

*CIR-h(t) output*: Finally, from the corrected channel transfer function $H(f)$, the new $h(t)$ is obtained via IFFT, and the last step is to perform the power scaling according to the path loss parameter. At the end of this process, the model generation is finished, and the $h(t)$ or Channel Impulse Response is ready to be used in any simulation tool.

### B. Soft-NLOS Case

Is the case when there is no direct path, but there is/are reflected path/s between Tx and Rx (i.e., metal cabinets). In this case the multi-cluster approach is needed.

*Cluster positioning*: In this case, many clusters will be considered. The first cluster may or may not be the strongest one, depending on the environment and the obstruction type for the direct path.

*CIR-h(t) complete response*: From each individual cluster and taking into account the randomly generated cluster arrival times and amplitudes, the complete response is directly obtained by the coherent addition of the different generated clusters. Zero padding at the beginning of the vector can be performed in order to simulate the first cluster delay due to the distance between the Tx and the Rx. Unless otherwise stated, the steps are the same as the LOS case.

### C. Hard-NLOS Case

This is the case where there are no direct or reflected paths between Tx and Rx (i.e., located in different rooms). The approach followed in this case is quite similar to the LOS case, with different parameters and attenuation factor in the power path loss law.

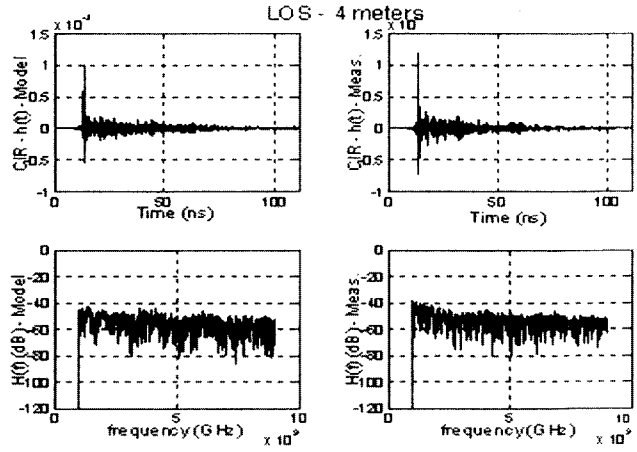


Fig. 18. LOS simulation vs. measurement.

*Cluster positioning*: As a first approximation, only one strong cluster will be considered.

### D. Corridor Case

This is a special case of LOS cases, happens when there is a direct path, but also when there are many strong reflected paths, thus, the multi-cluster approach is needed.

*Cluster positioning*: many clusters will be considered. The first cluster is the strongest one (the LOS direct path), and the other cluster amplitudes are a function of the environment.

*CIR-h(t) complete response*: From each individual cluster and taking into account the randomly generated cluster arrival times and amplitudes, the complete response is directly obtained by the coherent addition of the different generated clusters. Zero padding at the beginning of the vector can be performed in order to simulate the first cluster delay due to the distance between the Tx and the Rx.

## VII. SIMULATION AND EXAMPLES

Some examples from the four different cases modeled and explained in the previous section are presented in the following pages. The accuracy of the results can be visually checked through the comparison between the model realizations and the measured data, while the computed deviation between the statistical parameters extracted from the model realizations and the measurements is kept below 7 % of divergence. In all the cases a response duration of 400ns was considered and the time resolution fixed at 55 ps.

### A. LOS Case Example (4 m Distance Between Tx and Rx)

As it can be easily checked in Fig. 19, the first component is the most remarkable, simplifying the comparison with the measured data, where the match between the first components is clear, as well as the average behaviour in the $H(f)$.

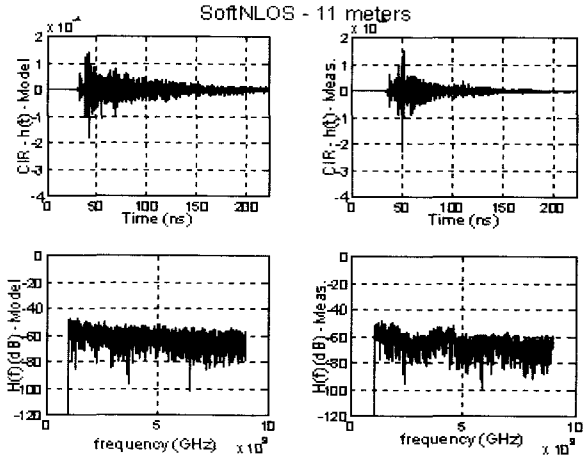


Fig. 19. Soft-NLOS simulation vs. measurement.

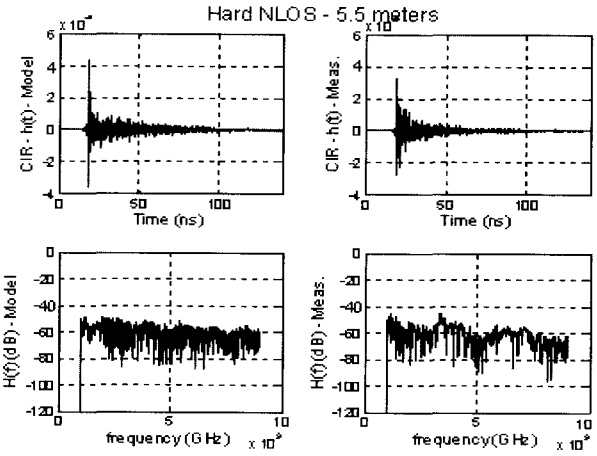


Fig. 20. Hard-NLOS simulation vs. measurement.

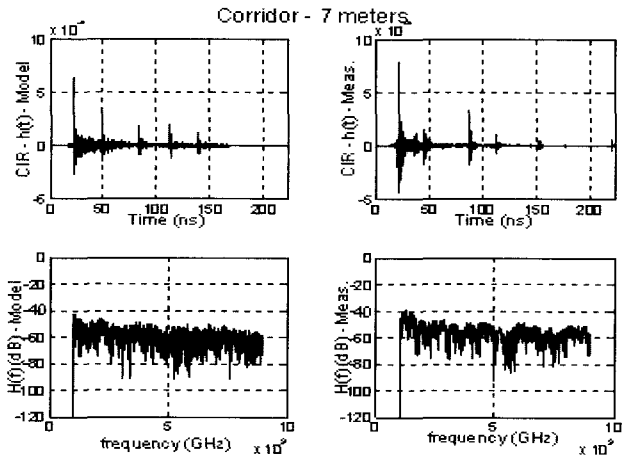


Fig. 21. Corridor simulation vs. measurement.

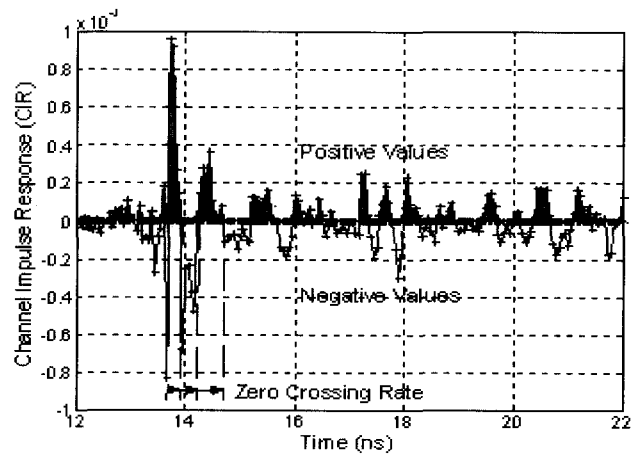


Fig. 22. Zero crossing rate representation.

### B. Hard-NLOS case Example (5.5 m Distance)

Once more the first component is the main one, there being in this case a similar behavior in the $H(f)$, but 5–7 dB lower on the average compared with the LOS case, due to the wall attenuation.

### C. Soft-NLOS Case Example (11m Distance)

In this example, the first component is neither the most remarkable nor the only one, since there are more components all along the response. Obviously, it does not match perfectly every detail, as it would be expected from a statistical model, but the tendency is clearly followed. The average level of $H(f)$ is matched, since it depends mainly on the distance.

### D. Corridor case Example (11m Distance)

As it can be seen in Fig. 21, the first component is the strongest one, but there are many other strong and emphasized path components along the $h(t)$ response, following both the measurements and the model, and following the same tendency from the statistical point of view. This means that for a single realization of the model, the result may differ for one particular measurement, but a set of model realizations will always fit the statistics of the measurements.

## VIII. CONCLUSION

The proposed channel model has achieved a high degree of accuracy, once compared with the measured data, in all the four different scenarios covered by this report. The values for the statistical parameters extracted from several realizations of the model fit up to a 93 The flexibility of the model, enabling the right matching of very different environment statistics, offers many advantages for designers at the system simulation stages. New measurement methodologies, as well as data post-processing techniques for UWB systems, have been developed during this research, driven by the design requirements and the particular features of this technology. The model has proven to be more accurate once the new parameters were considered. The inherent increment in the computational burden can be neglected when considering the new, and powerful, simulation platforms available in any laboratory.

## REFERENCES

[1] M. Win and R. Scholtz, "Impulse radio: How it works," *IEEE Commun. Lett.*, vol. 2, no. 1, pp. 10–12, Jan. 1998.

[2] A. A. M. Saleh, R. A. Valenzuela, "A statistical model for indoor multipath propagation," *IEEE J. Select. Areas Commun.*, vol. 5, no. 2.

[3] H. Hashemi. "The indoor radio propagation channel," *Proc. IEEE*, July 1993, pp.943–968.

[4] L. Rusch *et al.*, "Characterization of UWB propagation from 2 to 8 GHz in a residential environment," *IEEE Trans. Veh. Technol.*, June 2002.
[5] P. Pagani *et al.*, "A study of the ultra-wide nand indoor channel: Propagation experiment and measurement results," in *Proc. IWUWBS'2003*, June 2003.
[6] S. S. Ghassemzadeh *et al.*, "A multipath intensity profile model for residential environments," in *Proc.* WCNC'2003, Mar. 2003.
[7] J. Kunisch and J. Pamp, "Radio channel model for indoor UWB WPAN environments," IEEE P802.15-02/281-SG3a., Sept. 4, 2002.
[8] V. Hovinen, M. Hämäläinen, and T. Pätsi, , "Ultra wideband indoor radio channel models: Preliminary results," in *Proc. Ultra Wideband Systems and Technology'2002*.
[9] J. Kunisch and J. Pamp, "Measurement results and modeling aspects for the UWB radio channel," in *Proc. Ultra Wideband Systems and Technology'2002*.
[10] S. Loredo , L. Valle, and RP. Torres, "Accuracy analysis of GO/UTD radio channel modelling in indoor scenarios," *IEEE Antennas and Propagation Magazine*, vol. 43, no. 5, Oct. 2001.
[11] J. M. Cramer, R. A. Scholtz, and M. Z. Win, "Spatio-temporal diversity in ultrawideband radio," in *Proc. WCNC'99*, vol. 2, pp. 888–892.
[12] K. Bury, *Statistical Distributions in Engineering*, Cambridge University Press, 1999.
[13] W.C.Y., Lee, *Mobile Cellular Telecommunications Systems*, McGraw Hill Publications, New York, 1989.

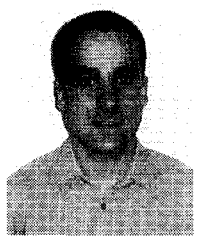

**Álvaro Álvarez** (S'02) was born in Oviedo, (Asturias), Spain in 1978. He received the M.S. degree in Telecommunications Engineering from the University of Cantabria, Cantabria, Spain, in 2002, and he developed his Master Project at the University of Kansas, Lawrence (KS), USA, under the supervision of Professor K. Sam Shanmugan (Southwestern Bell Distinguished Professor). He joined the R&D department of ACORDE.SA in June 2002, working in the field of WLAN systems, sensor networks and UWB communications. He is currently performing his Ph.D degree at the University of Cantabria, Cantabria, Spain, where he also works as Associate Professor of the Department of Communications Engineering, teaching Circuit Analysis and Circuit Simulation Tools. His current research interests include Impulse Radio systems, Localization Techniques and Wireless Smart Sensor Networks.

**Gustavo Valera** was born in Merida, Venezuela, in 1972. He received the System Engineer degree from the Universidad de los Andes, Márida, Venezuela, in 1999, and is currently working toward the PH.D. degree in electronic engineering at the Universidad de Cantabria, Santander, Spain. In 2001, He joined the Departamento de Ingeniería de Comunicaciones, Universidad de Cantabria. His research interests include the coexistence between Ultra-wideband devices and its consequences over the currently operational communications systems. Also, Ultra-wideband channel sounding, modeling and simulation.

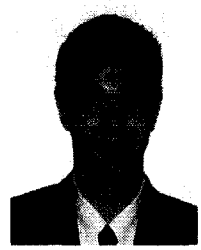

**Manuel Lobeira** (S'02) was born in Santander (Cantabria) Spain in 1977. He received the M.S degree in Telecommunications Engineering from University of Cantabria, Cantabria, Spain, in 2000. He is currently pursuing the Ph.D. in the field of Ultrawideband communications, in the same University, while collaborating with ACORDE in the design of RF/microwave systems for wireless applications. His research topics are: 1) WLAN, Propagation analysis and RF architecture design and development. 2) UWB, Channel characterization, implementation challenges and new access techniques.

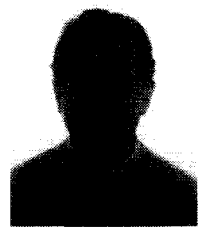

**Rafael Pedro Torres** (M'90) was born in Málaga, Spain, in 1961. He received his MS degree in Physics from the University of Granada (Spain) in 1986 and his Ph.D. from the Telecommunications Engineering School at the Polytechnic University of Madrid (UPM) in 1990. From 1986 to 1990 he was with the Radio Communication and Signal Processing Department of the UPM as a research assistant. During this time, he worked about numerical methods in electromagnetics, and its applications to design of passive microwave devices like radomes, circular polarizer, rotators and planar lenses. He became an associate professor in the Department of Communication Engineering of the University of Cantabria (Spain) in 1990. From this time to the present, he has participated in several projects about RCS computation, on board antennas analysis, electromagnetic compatibility, and radio-propagation. He is co-author of a book about the CG-FFT method, author of several chapters in different books, more than 20 papers, and about 80 conference contributions. He has been the leader of the group that has developed the code CINDOOR, Computer Tool for Planning and Design of Wireless Systems in Enclosed Spaces. His current research interests include radiopropagation for wireless and mobile communications, as well as the simulation and design of new wireless communications systems.

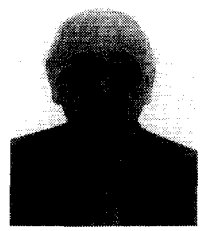

**Jose Luis Garcia** (M'74) was born in Zaragoza, Spain, in 1938. He received the M.S.E. Degree by the University of Zaragoza, Zaragoza, Spain, in 1964 and the Ph.D. by the University of Valladolid, Valladolid, Spain, in 1971. From 1966 to 1973, he was an Associate Professor at the University of Valladolid, where he was involved with analog systems simulation, and pseudorandom signal generation. In 1973, he became a Professor of Electronics Engineering in the Department of Electronics, University of Cantabria, Cantabria, Spain. He is currently the head of the Department of Communications Engineering at this University. He has been involved with microwave and millimeter-wave systems and components for mobile, radiolinks and satellite communications. His current research interests include broadcasting of digital TV through satellite and SMATV-DTM systems, wireless CDMA-SS for indoor applications, low-speed CDMA satellite communications, UWB communications and low-powered smart sensor networks. Dr. Gracia is a member of the Committee of the E-12 professional group of the Institute of Electrical Engineers (IEE), U.K.